Magnetic properties of iron-doped manganites

L. K. Leung,* A. H. Morrish, and B. J. Evans†
Department of Physics, University of Manitoba, Winnipeg, Canada, R3T 2N2
(Received 16 December 1975)

Polycrystalline samples of $La_{1-x}Pb_xMn_{1-y}{}^{57}Fe_yO_3$ with $0.20<x<0.45$ and $0.03\leqslant y\leqslant 0.17$ have been made and characterized by x-ray and wet chemical analysis. Earlier, it had been established that manganites with $y=0$ and $0.25<x<0.45$ are ferromagnets with a narrow double-exchange band providing the dominant coupling. The introduction of iron reduces the magnetization and the Curie temperature and also changes the shape of the magnetization versus temperature curve. Mössbauer spectra with and without an external magnetic field of 50 kOe imply that an iron ion with only Mn nearest neighbors has its spin almost antiparallel to the manganese magnetization. However, when two or more iron ions are adjacent, their spins make angles of about 55° to the direction of the net magnetization. From the isomer shift, it follows that the iron ions are in the high-spin Fe^{3+} state. The data are interpreted in terms of a model that considers the antiferromagnetic Fe-O-Mn and Fe-O-Fe superexchange interactions in addition to the ferromagnetic Mn^{3+}-Mn^{4+} double-exchange interaction.

INTRODUCTION

Earlier studies in our laboratory have shown that manganites with the chemical formula $La^{3+}_{1-x}Pb^{2+}_xMnO_3$ are ferromagnets for $0.25<x<0.45$. The Curie temperatures T_f are above room temperature ($320<T_f<350$ K), and the spontaneous magnetization at absolute zero corresponds to complete ferromagnetic ordering of the Mn^{3+} and Mn^{4+} spin system.[1,2] The origin of the ferromagnetism is thought to be a coupling produced by a narrow double-exchange band. Theories have been developed that describe the experimental data well.[3] As an extension to this work, compounds in which some manganese is replaced by iron enriched in the isotope ^{57}Fe have been made. Both the magnetization and Mössbauer spectra have been determined as a function of temperature.

The concept of the double-exchange interaction was introduced and developed during the past quarter century in order to account for the ferromagnetism of certain semiconducting compounds.[4] For the $La_{1-x}Pb_xMnO_3$ series, the Mn^{3+} ions can contribute $1-x$ electrons per manganese ion to the narrow conduction band. The coupling between the Mn^{4+} ions, which have a $3d^3$ configuration, then occurs via the itinerant electrons. The situation will however be changed when some manganese is replaced by iron. The d electrons of an Fe^{3+} ion are known to be more localized than those of a Mn^{3+} ion,[5] and as a result superexchange interactions may exist. The manganites doped with iron therefore provide a system in which the interplay between localized and collective electron behavior may, in principle, be studied.

SAMPLE PREPARATION AND CHARACTERIZATION

Although single crystals grown by the flux technique had been employed for the previous experiments on $La_{1-x}Pb_xMnO_3$, the cost of enriched iron dictated that only small polycrystalline samples of the iron doped materials be made. Therefore, amounts of the oxides (PbO, MnO_2, Mn_2O_3, La_2O_3, and $^{57}Fe_2O_3$) appropriate to the chemical formula, $La_{1-x}Pb_xMn_{1-y}Fe_yO_3$ desired, were intimately mixed by wet grinding an acetone slurry. The ranges of composition were $0.20<x<0.45$ and $0.03\leqslant y\leqslant 0.17$. Iron oxide enriched with 92.8% of the isotope ^{57}Fe was used. The mixtures of powders were pressed into pellets and fired at 800 °C in a top-loaded furnace. The pellets were quenched in air, ground to a fine powder, repelleted, and refired at 1000–1200 °C; this procedure was repeated until x-ray powder patterns showed that all the samples were single phase.

Samples were also made by slow cooling in the furnace. Then, Mössbauer spectra possessed an additional pattern which had a hyperfine splitting at room temperature, close to, but somewhat larger than, that for pure iron. Presumably some iron ions were tending to bond together to form clusters. Consequently, all the samples investigated further were formed by quenching from temperatures above 900 °C. However, the particle sizes in the samples were only about 1 μm. These small sizes led to other complications, as will become apparent later.

The lattice constants were determined with a Philips 57.3-mm radius Debye-Scherrer camera and diffractometer using both Mn-filtered Fe $K\alpha$ and Ni-filtered Cu $K\alpha$ radiation. As an example,

TABLE I. Powder diffraction data for $La_{0.74}Pb_{0.26}Mn_{0.90}Fe_{0.10}O_3$.

Intensity	d_{obs}	d_{calc}	hkl
60	3.902	3.902	200
100	2.772	2.772	$2\bar{2}0$
100	2.745	2.747	220
10	2.354	2.362	$1\bar{3}1$
40	2.258	2.260	$22\bar{2}$
30	2.232	2.232	222
80	1.949	1.951	040
30	1.750	1.751	$04\bar{2}$
30	1.736	1.739	240
70	1.595	1.600	$24\bar{2}$
		1.595	$24\bar{2}$
50	1.580	1.581	242
50	1.385	1.386	$04\bar{4}$
50	1.373	1.373	440
30	1.306	1.306	$24\bar{4}$
30	1.300	1.301	060
10	1.292	1.290	442
40	1.237	1.237	$06\bar{2}$
40	1.230	1.230	260
10	1.182	1.181	$\bar{6}22$
20	1.178	1.177	$62\bar{2}$
10	1.169	1.170	622
20	1.130	1.130	$44\bar{4}$
20	1.116	1.116	444
20	1.087	1.087	$\bar{6}40$
10	1.078	1.078	640

the complete powder diffraction data for $La_{0.74}Pb_{0.26}Mn_{0.90}Fe_{0.10}O_3$ are listed in Table I. The structure is that of a rhombohedrally distorted perovskite. The presence of the $1\bar{3}1$ line indicates a doubling of the cell edges. The lattice constants for all the samples are recorded in Table II. They do not seem to follow any regular pattern as a function of x or y. The iron-doped manganites have, therefore, the same structural characteristics as the undoped samples.[1]

TABLE II. Lattice constant of $La_{1-x}Pb_xMn_{1-y}Fe_yO_3$.

x	y	a_{rh} (Å)	α_{rh}
0.44	0.03	7.761 ± 0.001	90°45′ ± 3′
0.44	0.05	7.763 ± 0.001	90°28′ ± 3′
0.44	0.10	7.773 ± 0.001	90°17′ ± 3′
0.44	0.14	7.789 ± 0.005	90°33′ ± 5′
0.44	0.17	7.794 ± 0.004	90°45′ ± 5′
0.14	0.10	7.777 ± 0.020	90°30′ ± 5′
0.20	0.10	7.793 ± 0.008	90°41′ ± 3′
0.26	0.10	7.798 ± 0.002	90°30′ ± 3′
0.44	0.10	7.773 ± 0.001	90°17′ ± 3′
0.55	0.10	7.775 ± 0.005	90°48′ ± 4′
0.65	0.10	7.773 ± 0.003	90°46′ ± 3′
0.30	0.03	7.821 ± 0.001	90°35′ ± 3′
0.30	0.10	7.797 ± 0.001	90°34′ ± 3′
0.30	0.15	7.797 ± 0.001	90°27′ ± 3′

A search was made for the presence of other phases by examining powder patterns taken with lengthy exposure times. Very weak additional lines were observed and identified as unreacted La_2O_3, and which constituted about 1% of the final sample. In order to test for stoichiometry, the amount of manganese in different valence states was determined by wet-chemical analyses of two selected samples.[6] There was no Mn^{2+} present. The chemical formulas implied by the wet analyses were $La_{0.70}Pb_{0.30}Mn^{3+}_{0.672}Mn^{4+}_{0.298}Fe_{0.03}O_3$ and $La_{0.70}Pb_{0.30}Mn^{3+}_{0.610}Mn^{4+}_{0.290}Fe_{0.10}O_3$, which agree, within the experimental error, with the assumed formulas $La_{0.70}Pb_{0.30}Mn^{3+}_{0.67}Mn^{4+}_{0.30}Fe_{0.03}O_3$ and $La_{0.70}Pb_{0.30}Mn^{3+}_{0.60}Mn^{4+}_{0.30}Fe_{0.10}O_3$, respectively. It can be concluded with some confidence that the desired total oxidation state had been achieved.

MAGNETIZATION BELOW T_f

The magnetization of a few typical samples was determined with a Foner vibrating-sample magne-

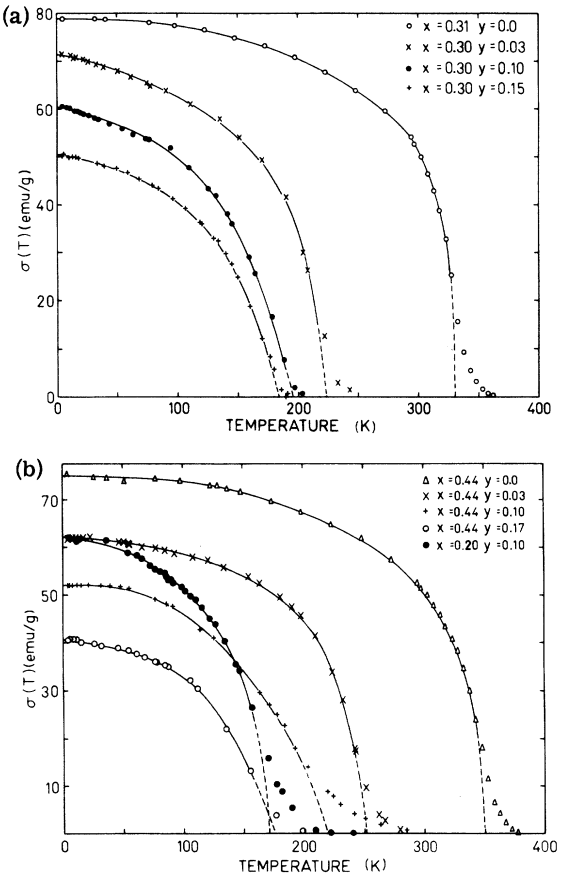

FIG. 1. Saturation magnetization as a function of temperature for $La_{1-x}Pb_xMn_{1-y}Fe_yO_3$, (a) with $x=0.30$ and 0.31, and (b) with $x=0.20$ and 0.44.

TABLE III. Curie temperature and spontaneous magnetization of $La_{1-x}Pb_xMn_{1-y}Fe_yO_3$.

x	y	T_f (K) (expt)	T_f (K) (theor)	$\sigma(0)$ (emu/g) (expt)	$\sigma(0)$ (emu/g) Spin configuration (1)	(2)	(3)
0.31	0	330	330	78.8	78.5	78.5	
0.30	0.03	224	224	71.4	73.0	73.5	73.6
0.30	0.10	196	196	60.5	59.6	64.6	65.5
0.30	0.15	184	184	50.7	50.0	59.9	64.0
0.44	0	350	350	74.8	73.2	73.2	
0.44	0.03	252	234	61.9	67.5	68.1	
0.44	0.10	220	199	52.1	54.6	59.4	
0.44	0.17	176	174	40.7	41.7	54.2	
0.20	0.10	172		62.0	62.4		

tometer from 4.2 K up to the Curie (or more precisely, the ferrimagnetic Néel) temperature T_f. The spontaneous magnetization was found by extrapolation to zero applied magnetic field, and the results are shown in Fig. 1. The Curie temperature was also determined by extrapolation procedures described earlier,[2] and are listed in Table III. Values of the spontaneous magnetization at $T=0$ K, $\sigma(0)$, found by extrapolation are also tabulated.

The spontaneous magnetization differs as a function of temperature from that for the undoped compounds. To bring this point out, plots of reduced magnetization versus reduced temperature are shown in Fig. 2. Clearly, the curve becomes more Brillouin-like at first, and then as the iron concentration increases (15 at.%), decreases in slope, especially as T_f is approached. These results suggest immediately that the magnetization can no longer be understood by considering only the double-exchange mechanism.

At this point, it is instructive to see if the spontaneous magnetization at absolute zero corresponds to any simple spin configuration. Since the data seem to imply that the Fe-O-Mn superexchange interaction is antiferromagnetic, a simple structure is considered first in which all the iron ions (assumed to be in the high-spin Fe^{3+} state) are aligned antiparallel to the Mn^{3+}-Mn^{4+} system. It is also assumed that there is no orbital contribution. The calculated values of $\sigma(0)$ are then given in Table III in the column under *spin configuration (1)*. For $x=0.30$ the agreement with the experimental values is very reasonable; for $x=0.44$ it is much poorer. When the Fe^{3+}-O-Fe^{3+} antiferromagnetic superexchange interaction is considered as well, a more sophisticated model of the spin structure is easily developed from the following considerations. Each site occupied by a Mn or Fe ion, the bcc position at $\frac{1}{2}\frac{1}{2}\frac{1}{2}$, has six similar nearest-neighbor sites. The probability that an Fe^{3+} ion has n nearest-neighbor sites occupied by Fe ions is given by the binomial formula

$$P(n,y)=\binom{6}{n}y^n(1-y)^{6-n}, \tag{1}$$

where y is the iron concentration. At low iron concentrations the most likely arrangement is for $n=0$, that is, with all six nearest-neighbor sites occupied by Mn ions. By $y=0.15$, the probability is about equal for six-Mn or for five-Mn–one-Fe nearest-neighbor configurations [actually $P(0,0.15)=0.377$, $P(1,0.15)=0.399$, and $P(2,0.15)=0.176$]. As a second approximation, therefore, consider a model in which Fe^{3+} ions with six Mn ions as nearest neighbors are antiparallel, and Fe^{3+} ions with one or more Fe^{3+} ions as nearest neighbors are perpendicular, to the spins of the manganese system. The spontaneous magnetizations predicted at $T=0$ K are listed under the column *spin config-*

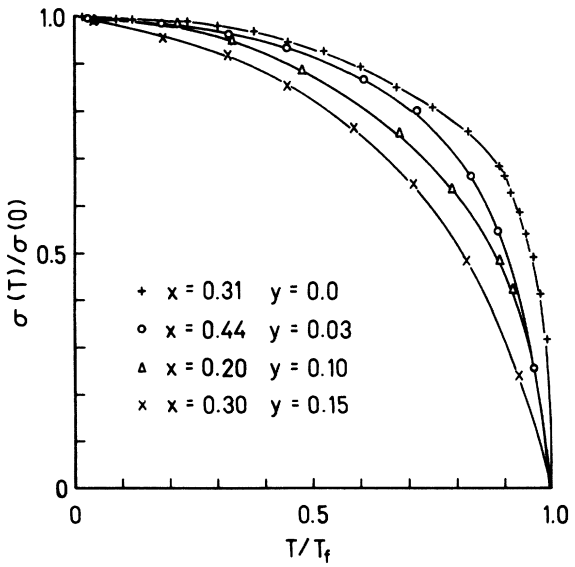

FIG. 2. Magnetization of the iron-doped manganites vs temperature in reduced units.

uration (2) in Table III, and provide a poorer fit with experiment than *spin configuration (1)*. At this point it is useful to consider the information that can be deduced from Mössbauer spectra, and to return later to the discussion of the magnetization data.

MÖSSBAUER SPECTRA AND ANALYSIS

The Mössbauer spectra were obtained with a constant-acceleration transducer and a multichannel analyzer operated in the time mode. Most of the data were collected at 7 K, with and without a magnetic field. A few spectra were taken between liquid-nitrogen temperature to just above T_f. In addition, several spectra were obtained at room temperature where all the samples were paramagnets, and a small number at temperatures

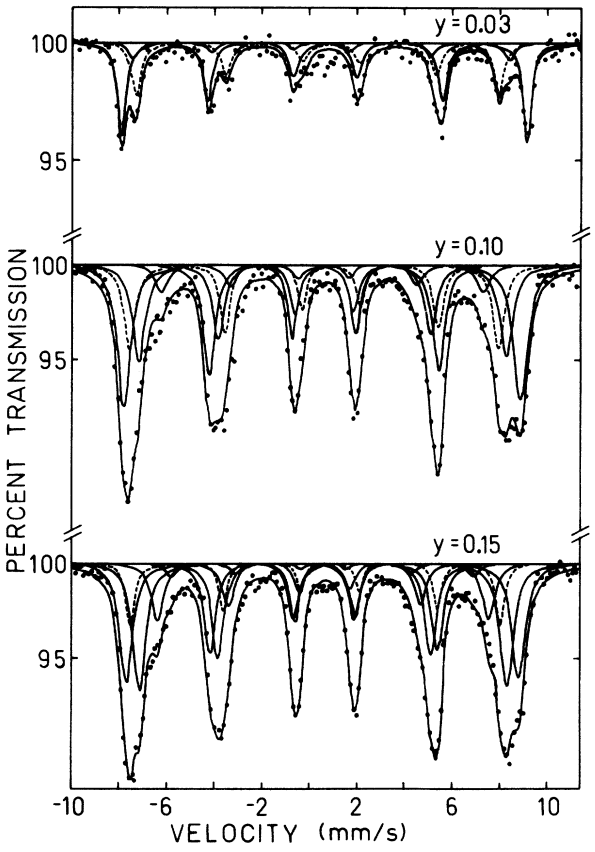

FIG. 3. Mössbauer spectra for $La_{0.70}Pb_{0.30}Mn_{1-y}Fe_yO_3$ at 7 K and in zero external magnetic field. The points represent the experimental data and the curves the individual patterns and their sum obtained by a computer fit. The intensities of the lines are constrained to be proportional to the probabilities $P(n,y)$, where n is the number of iron nearest neighbors. In addition, the lines were assumed to be Lorentzian and width constraints were applied.

TABLE IV. Mössbauer data for $La_{0.70}Pb_{0.30}Mn_{1-y}Fe_yO_3$ at 7 K. The subscript s refers to iron ions near the surface, and the subscripts 0, 1, 2, 3 to the value of n, the number of iron nearest neighbors. The isomer shifts δ are with respect to chromium. The intensities I give the % absorption compared to background transmission. The magnetic fields H are in kOe, and all other Mössbauer parameters in mm/sec.

y	H_{ext}	H_s	H_0	H_1	H_2	H_3	I_s	I_0	I_1	I_2	$\Gamma_{1,6_s}$	$\Gamma_{1,6}(0-3)$	δ_s	δ_0	δ_1	δ_2	δ_3	$\frac{1}{4}e^2qQ_s$	$\frac{1}{4}e^2qQ_0$	$\frac{1}{4}e^2qQ_1$	$\frac{1}{4}e^2qQ_2$	$\frac{1}{4}e^2qQ_3$
0.03	0	474	528	488	430		0.023	0.039	0.002	0.003	0.49	0.49	0.64	0.66	0.58	0.75		−0.29	−0.01	−0.02	0.00	
0.10	0	482	517	481	423		0.072	0.074	0.028	0.024	0.61	0.61	0.59	0.61	0.64	0.64		−0.29	−0.04	0.03	−0.02	
0.15	0	481	511	475	422		0.075	0.063	0.041	0.025	0.67	0.67	0.61	0.64	0.69	0.64		−0.23	−0.02	0.09	−0.02	
0.03	0	472	528	491	458		0.022	Constrained to			0.52	0.44	0.66	0.66	0.53	0.90		−0.29		−0.018		
0.10	0	480	515	478	419	389	0.043	value of $P(n,y)$			0.57	0.66	0.58	0.60	0.61	0.59	0.49	−0.36		−0.033		
0.15	0	483	512	480	433	395	0.032	[Eq. (1)]			0.45	0.65	0.61	0.63	0.65	0.64	0.60	−0.31		−0.024		
0.03	50	511	567	480	427		0.021	0.055	0.004	0.005	0.46	0.46	0.60	0.67	0.62	0.69		−0.22				
0.10	50	513	555	454	401		0.059	0.087	0.024	0.023	0.79	0.79	0.56	0.54	0.53	0.61		−0.19				
0.15	50	510	553	452	398		0.046	0.073	0.042	0.023	0.83	0.83	0.59	0.58	0.64	0.59		−0.14				

TABLE V. Parameters deduced from Mössbauer data for $La_{0.70}Pb_{0.30}Mn_{1-y}Fe_yO_3$ at 7 K.

y	n (or s surface)	$P(n,y)$ (%) Eq. (1)	I (%) $H_{ext}=0$	I (%) $H_{ext}=50$ kOe	H_{hf} (kOe) $H_{ext}=50$ kOe	θ (deg) Eq. (2)	H_{hf} (kOe) Eq. (3)
0.03	s				511	146.6	516
0.03	0	83.3	81.4	81.4	567	160.3	578
0.03	1	15.5	12.9	7.4	480	71.0	474
0.03	2	1.2	5.7	11.2	427		
0.10	s				513	144.6	523
0.10	0	53.1	53.5	55.7	555	160.4	564
0.10	1	35.4	26.8	22.1	454	52.0	452
0.10	2	9.8	19.7	22.2	401	56.3	397
0.15	s				510	134.0	517
0.15	0	37.7	48.6	44.1	553	165.4	558
0.15	1	39.9	30.9	35.9	452	53.2	451
0.15	2	17.6	20.5	20.0	398	55.6	394

above room temperature up to about 700 K.

The Mössbauer spectra at 7 K for $x=0.30$ and $y=0.03$, 0.10, and 0.15 are shown in Fig. 3. The spectra were fitted with up to five six-line patterns by the method of least squares using an IBM 360/65 computer. All lines were assumed to have a Lorentzian shape and widths that satisfied the condition $\Gamma_i=\Gamma_{7-i}$, where i represents the line number (1–6) and Γ_i is the same for all patterns of a given spectra.

One of the patterns (shown as the dashed lines in Fig. 3) was a conundrum for a time. The possibility that the pattern is to be associated with iron ions that have replaced Pb or La ions in the lattice seems unlikely from radius ratio considerations. An enhancement of this pattern in the paramagnetic regime is found when a back-scatter Mössbauer geometry was employed.[7] It appears therefore that the pattern is to be attributed to iron ions that are associated with an oxygen vacancy, there being a larger concentration of such defect structures at the surface than in the bulk. Presumably the pattern has an appreciable intensity because the particle sizes in our samples are so small (~ 1 μm).

The remaining patterns may be related to the ionic distributions of the iron and manganese, assumed to be random. If so, their areas (or their intensities, in view of the width constraints) should be in the same ratio as the probabilities $P(n,y)$ given by Eq. (1). A computer fit with only line shape and width constraints gave values for the hyperfine fields, quadrupole interactions ($\frac{1}{4}e^2qQ$), isomer shifts δ, outer linewidths ($\Gamma_1=\Gamma_6$), and outer line intensities that are listed in Table IV. The areas (intensities) of the different patterns, normalized and expressed as a percent, are given in Table V. They are in respectable accord with the values of $P(n,y)$, which are also tabulated in Table V. A further computer fit was made with the intensity constraints for each pattern corresponding to the probabilities $P(n,y)$. The values of the goodness of fit parameter χ^2 were no worse than those obtained when the intensities were unconstrained. The individual patterns computed with intensity constraints, together with the sum of all patterns, are plotted in Fig. 3 as full curves.

Mössbauer spectra taken with a magnetic field

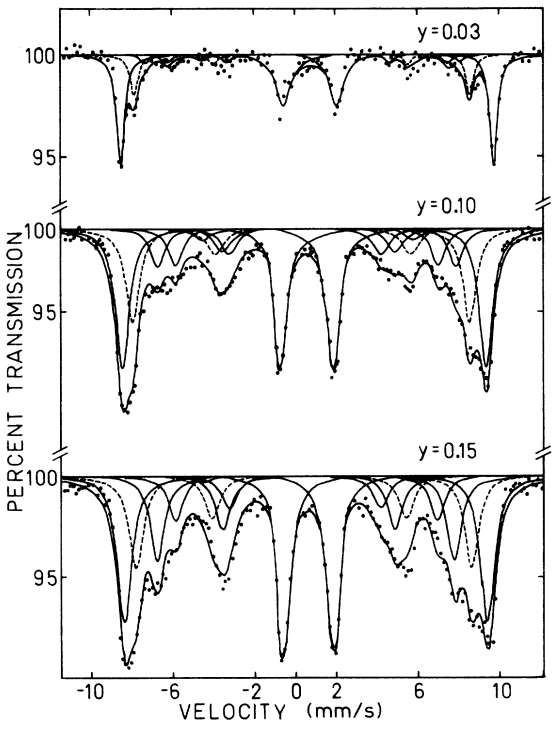

FIG. 4. Mössbauer spectra for $La_{0.70}Pb_{0.30}Mn_{1-y}Fe_yO_3$ at 7 K in an external magnetic field of 50 kOe applied parallel to the direction of propagation of the γ ray. No intensity constraints were placed on the individual patterns, indicated by the curves.

of 50 kOe applied along the direction of propagation of the γ ray are shown in Fig. 4 for the same samples of Fig. 3. The spectra were fitted with overlapping six-line patterns with the same line shape and width constraints used for the zero-field data. These patterns are drawn in Fig. 4, with the same conventions as for Fig. 3. The various parameters deduced are also listed in Table IV. In addition the relative outer line intensities are given in Table V; the agreement with $P(n, y)$ is close enough to justify considerable confidence in the pattern identifications.

The presence of the 2–5 lines in Fig. 4 implies that the iron spin structure is not collinear with the direction of the applied magnetic field, and hence the magnetization of the manganese system. Further, the increase in the hyperfine fields for the two patterns identified with ions near the surface and with $n=0$ establishes that these ions have an appreciable component of their electronic magnetic moment aligned antiparallel to the magnetization of the manganese ions. The other patterns exhibit a small decrease in hyperfine fields, and therefore the associated iron ions have moments with a small component parallel to the manganese magnetization.

For the experimental geometry used, the average angle Θ between the direction of the applied field and the hyperfine field at an iron ion associated with a particular pattern is given by

$$\Theta = \arcsin\left\{\tfrac{3}{2}\,(A_{2,5}/A_{1,6})/\left[1+\tfrac{3}{4}(A_{2,5}/A_{1,6}]\right\}^{1/2}, \tag{2}$$

where $A_{2,5}$ and $A_{1,6}$ are the areas of lines 2 or 5 and 1 or 6, respectively. The values of Θ found are given with respect to the direction of the applied field in Table V. Because the trigonometric function depends quadratically on the area $A_{2,5}$, and because the spectra are complex, it is possible that the angle for the pattern with $n=0$ may be close to or even equal to 180°; it is unlikely that the angle with the field axis is much greater than 20° (less than 160° with the field direction).

The hyperfine field in the presence of the external field, $H_{\rm hf}(H_{\rm ext})$ is given by

$$H_{\rm hf}(H_{\rm ext}) = [H_{\rm hf}(0)^2 + H_{\rm ext}^2 \pm 2H_{\rm hf}(0)H_{\rm ext}\cos\Theta]^{1/2}, \tag{3}$$

where $H_{\rm hf}(0)$ is the hyperfine field in zero external field and $H_{\rm ext}$ is the external field. The values of $H_{\rm hf}(H_{\rm ext})$ calculated for $H_{\rm ext}=50$ kOe and the Θ's determined from Eq. (2) are also listed in Table V. The agreement with the hyperfine fields determined from the computer-fitted patterns of Fig. 4 (relisted in Table V is respectable. In these analyses, the demagnetizing and Lorentz fields have not been taken into account.

It is necessary to consider the difference in hyperfine fields of the various patterns for a compound with a fixed value of x and y. Reference to Figs. 3 and 4 and Table IV shows that for $x=0.30$ the hyperfine field decreases by 90–100 kOe when n, the number of nearest-neighbor iron ions, changes from 0 to 2. In ferrimagnetic insulators it is customary to account for such variations by considering the supertransferred contribution to the total hyperfine field. In this interaction, a transfer of spin density occurs from the d orbitals of the nearest-neighbor cations through the σ orbitals of the oxygen ions to the 4s orbitals of the iron ion under consideration, a mechanism closely related to the superexchange interaction. Since the electronic configurations of the neighboring cations are $3d^3$ and $3d^5$ for the Mn^{4+} and Fe^{3+} ions, respectively, an *increase* in the supertransferred hyperfine field would be expected as n increases. Therefore, the observed decrease must be related to local fluctuations in the interaction between the double-exchange electrons and the 4s orbital of the Fe ion when it has one or more iron nearest neighbors. In other words, the 4s polarization produced by the highly polarized itinerant band electrons of the Mn^{3+}-Mn^{4+} system must be significantly decreased by the perturbation caused when two or more iron ions are nearest cation neighbors. Any other contribution to the hyperfine field does not appear to be capable of producing the decrease observed.

The isomer shifts given in Table IV are well within the range observed for high-spin ferric ions, and hence strongly support the earlier assumptions. The quadrupole shifts are small, except for the pattern identified with iron ions near the grain surfaces. It is reasonable to expect that the electric field gradient will be larger for these ions.

A more ambitious analysis of the spectra at 7 K and with no external field applied will now be made by considering also the magnetic cations on the 12 next-nearest neighbor sites. The hyperfine field at a particular ^{57}Fe nucleus will be assumed to be given by

$$H(n,m) = H_0(1+na+mb), \tag{4}$$

where n is the number of nearest iron-ion neighbors, m is the number of next-nearest iron-ion neighbors, and H_0 is the hyperfine field for n and m equal to zero. The following constraints were applied: (i) The linewidths for each line of the pattern for the surface ions were set equal. (ii) The line intensities for the surface-ion pattern were fixed according to a previously determined area ratio. (iii) The linewidths Γ_0, isomer shifts

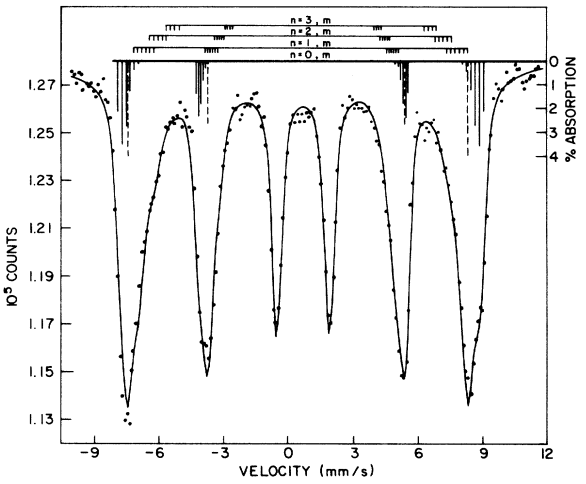

FIG. 5. Mössbauer spectrum for $La_{0.70}Pb_{0.30}Mn_{0.85}Fe_{0.15}O_3$ at 7 K fitted with 22 six-line patterns; their sum is shown by the full curve. The peak positions for the different patterns are indicated by the vertical bars. The dashed bars are for the surface-ion pattern. The other bars are for patterns associated with n Fe ions in the first (nearest-neighbor) coordination sphere, and m Fe ions in the second (next-nearest-neighbor) coordination sphere. For $n=0$, the percent absorption compared to background is indicated by the length of the bars and the scale at the right-hand side.

δ_0, and quadrupole shifts $\frac{1}{4}e^2qQ_0$ for all other patterns were individually held constant, that is, there was one value of each parameter for all patterns. (iv) The relative line intensities for these other patterns were kept proportional to the probabilities

$$P(n,m,y_{\text{eff}})=P(n,y_{\text{eff}})P(m,y_{\text{eff}})$$
$$=\binom{6}{n}y_{\text{eff}}^{n}(1-y_{\text{eff}})^{6-n}\binom{12}{m}y_{\text{eff}}^{m}(1-y_{\text{eff}})^{12-m}, \quad (5)$$

where $y_{\text{eff}}=y-y_s$, and y_s is the number of Fe ions associated with oxygen deficiencies per chemical formula unit. (v) All lines were Lorentzian in shape.

The spectrum for $y=0.03$ was fitted with 10 six-line patterns, that for $y=0.10$ with 17 six-line patterns, and that for $y=0.15$ with 22 six-line patterns ($x=0.30$). The sum of the individual patterns for the sample with $y=0.15$ is shown as the solid curve in Fig. 5; for all the spectra excellent values for χ^2 were obtained. The vertical bars indicate the peak positions for lines 1, 2, 5, and 6 of the individual patterns, dashed for the surface ion pattern, and solid for the others. The $m=0$ pattern has the largest splitting, and as m increases the splitting decreases. For $n=0$, the relative absorptions are indicated by the length of the bar.

The values of the various parameters deduced from the fittings are tabulated in Table VI. The relative intensities of the lines of each pattern are close to the 3:2:1 ratios predicted by the Clebsch-Gordan coefficients for an ideal Mössbauer absorber. It should be noted that the linewidths are significantly narrower than those given in Table IV, whereas the isomer shifts and the quadrupole shifts are substantially the same. It is encouraging that the value of H_0 is almost independent of y. The changes in $H(n,m)$, ΔH_1, when n changes by 1, and ΔH_2, when m changes by 1, obtained by using the values deduced for a and b, are also tabulated for each sample in Table VI. The major conclusion of the analysis is that when a manganese ion is replaced by an iron ion in the first coordination sphere (nearest neighbor), the hyperfine field decreases by about 48 kOe, and when a manganese ion is replaced by an iron ion in the second coordination sphere (next-nearest neighbor) the hyperfine field is decreased by about 17 kOe, essentially independent of the doping concentration.

The Mössbauer spectra between liquid-nitrogen temperature and the Curie point have broadened lines. Because the resolution of the patterns was relatively poor, only the average hyperfine fields were determined. These are plotted in reduced units in Fig. 6. The data points lie close to a Brillouin curve for $S=\frac{5}{2}$.

A Mössbauer spectrum at room temperature is shown for one compound ($x=0.30$, $y=0.03$) in Fig. 7. The spectra change but little up to $T\approx 700$ K, and with composition. Two doublets have been used to fit the spectra, and are also indicated in

TABLE VI. Mössbauer data for $La_{0.70}Pb_{0.30}Mn_{1-y}Fe_yO_3$ at 7 K assuming nearest-neighbor plus next-nearest-neighbor interactions. The isomer shifts δ are with respect to chromium. The magnetic fields, H and ΔH, are in kOe, and the other Mössbauer parameters, Γ, δ, and $\frac{1}{4}e^2qQ$, are in mm/sec. The intensity I_s is the absorption relative to the background for lines 1 or 6 for iron ions near the surface. The parameters a and b are defined in Eq. (4).

y	H_s	H_0	I_s	Γ_s	Γ_0	δ_s	δ_0	$\frac{1}{4}e^2qQ_s$	$\frac{1}{4}e^2qQ_0$	a	b	ΔH_1	ΔH_2
0.03	474	529	0.021	0.38	0.43	0.67	0.66	−0.32	−0.01	−0.095	−0.037	51	19
0.10	482	527	0.039	0.45	0.43	0.60	0.61	−0.36	−0.04	−0.088	−0.032	47	17
0.15	490	527	0.040	0.53	0.42	0.66	0.64	−0.19	−0.03	−0.087	−0.023	46	12

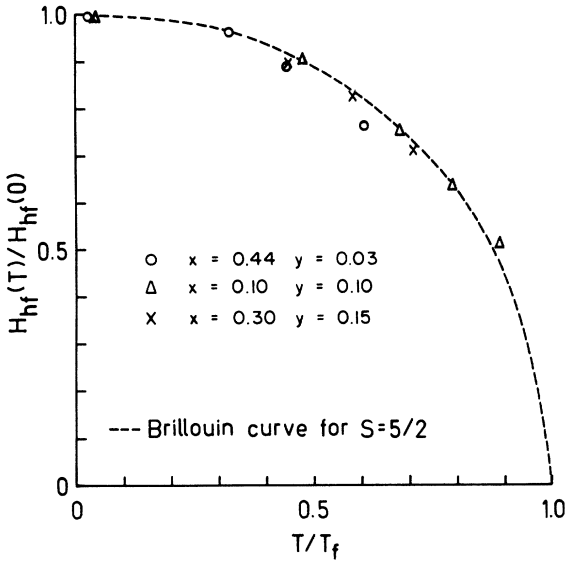

FIG. 6. Average hyperfine field at ^{57}Fe nuclei as a function of temperature in reduced units for $La_{1-x}Pb_x Mn_{1-y}Fe_yO_3$.

Fig. 7. The inner doublet has a quadrupole splitting of 0.236 mm/sec, an isomer shift of 0.54 mm/sec, and a linewidth of 0.40 mm/sec. The outer doublet has a quadrupole splitting of 1.55 mm/sec, an isomer shift of 0.54 mm/sec relative to chromium, and a linewidth of 0.31 mm/sec. This doublet may safely be attributed to the iron ions associated with a defect structure, e.g., an oxygen vacancy, for the following three reasons. First, this pattern has an enhanced relative intensity when a spectra is obtained with a backscatter geometry using the conversion electrons. A larger concentration of Fe ions with missing nearest neighbor oxygen ions is expected closer to the surface than in the bulk of the material. Second, the quadrupole splitting of 1.55 mm/sec for $|\frac{1}{2}e^2qQ|$, together with the average value of 0.29 mm/sec for $|\frac{1}{4}{}^2qQ\frac{1}{2}(3\cos^2\Theta - 1)|$ obtained for the magnetically ordered phase (Table IV or VI), yields the value $\Theta = 140°$, which is in very good agreement with the value $\Theta = 146°$ determined from the spectra in an applied field at 7 K (Table V). Here it has been assumed that the easy direction of the magnetization and the z axis for the electric field gradient both lie along the [001] direction. Third, the relative intensity of this doublet compares respectably with that for the corresponding pattern in the spectra at 7 K.

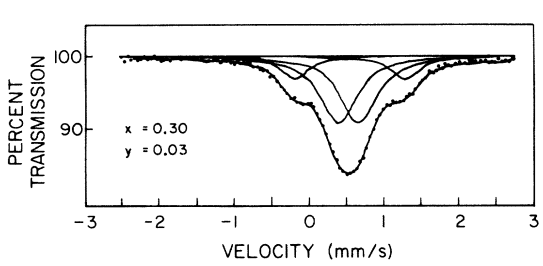

FIG. 7. Mössbauer spectrum at room temperature for $La_{0.70}Pb_{0.30}Mn_{0.97}Fe_{0.03}O_3$. Two quadrupole-split patterns are fitted.

FURTHER DISCUSSION

The magnetic structure for the iron ions, deduced from the Mössbauer spectra, has implications for the magnetization at absolute zero. Values of $\sigma(0)$ calculated using the angles (θ) of Table V, are listed in Table III under the column *spin configuration (3)* for the samples with $x = 0.30$. These values are somewhat larger than those for *spin configuration (2)*. It is necessary therefore to conclude that the manganese system is also noncollinear. The actual structure may be complex; it seems likely that manganese ions with one or more iron ions as nearest neighbors would cant at the largest angles. The investigation of the manganese spin structure by neutron-diffraction techniques is an experiment that may be of interest sometime in the future.

It is instructive to develop an energy diagram for the iron-doped manganites. A broad filled valence band is formed by the s- and p-bonding orbitals of the anions and cations. The antibonding

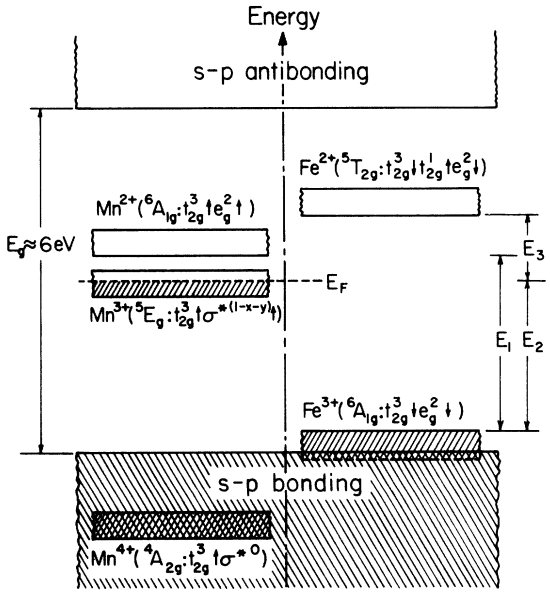

FIG. 8. Proposed energy-level diagram for $La_{1-x}Pb_x Mn_{1-y}Fe_yO_3$. The localized-electron manifolds are shown as a single energy. The cross hatching indicates occupied states.

s and p orbitals form a broad conduction band which is completely empty. The energy separation of these two bands E_g in oxides is typically about 6 eV. For clarity, the $3d$ electron manifolds of the different ions will be indicated as a single energy in the diagram, as shown in Fig. 8. The $3d$ electrons at the Mn ions consist of localized t_2 electrons and delocalized e electrons, all with parallel spins at absolute zero. There are $1-x-y$ electrons per chemical formula unit occupying the narrow double-exchange band σ^* formed by the e_g orbitals of the manganese ions. The Fe^{3+} ions form a well localized ${}^6A_{1g}$ state which lies below the fermi energy E_F. Now, the superexchange interaction would be ferromagnetic if a transfer of an e_g electron from a Fe^{3+} ion to a Mn^{3+} or Mn^{4+} ion was involved. However, this interaction is known to be antiferromagnetic. Therefore, the dominant electron transfer is from a Mn^{3+} ion to a Fe^{3+} nearest neighbor, since then the spin of the promoted Mn^{3+} electron will be antiparallel to the net spin of a Fe^{2+} ion. It follows that the empty ${}^5T_{2g}$ level of a Fe^{2+} ion lies close to but above the fermi level of the narrow σ^* conduction band. Also, the ${}^6A_{1g}$ level of a Mn^{2+} ion probably has only slightly greater energy than the ${}^5E_g$ level for Mn^{3+}. Since, from Fig. 8, $E_3 < E_2 < E_1$, it is clear that then the energy for a $Mn^{3+} + Fe^{3+} \rightarrow Mn^{4+} + Fe^{2+}$ electron transfer is much less than for either a $Mn^{3+} + Fe^{3+} \rightarrow Mn^{2+} + Fe^{4+}$ or a $Mn^{4+} + Fe^{3+} \rightarrow Mn^{3+} + Fe^{4+}$ transfer.

As an example of the use that can be made of the proposed energy-level diagram, an attempt will now be made to calculate the Curie temperatures of the iron-doped manganites. For the undoped compounds, the only interaction that will be considered is that of double exchange; the Curie temperature will be assumed to be related to the transfer integral t by the relationship

$$T_f = k_1 t z_{Mn} , \qquad (6)$$

where z_{Mn} is the average number of manganese nearest neighbors to a manganese ion ($z_{Mn} = 6$ here), and k_1 is a constant. From Table III, the experimental value for T_f for $x = 0.31$ yields $k_1 t = 55$. For the doped compounds, the double-exchange interaction will be reduced by the ratio of the number of itinerant electrons in the doped compounds to that for the undoped compounds, viz. $1 - y/(1-x)$. Also, the transfer integral itself will probably be reduced by the fraction f multiplied by the number of manganese ions per formula unit $(1-y)$. In addition, there will be superexchange interactions acting, primarily the type Fe-O-Mn, but also, to a lesser degree, the type Fe-O-Fe. Although these two interactions will be different, they will be lumped together in this analysis, and be denoted by $k_2 J$. Therefore, an approximate expression for the Curie temperature of the doped samples is given by

$$T_f = k_1 t z_{Mn} [1 - y/(1-x)](1-y) f + 12 y k_2 J , \qquad (7)$$

where the factor 12 in the second term on the right-hand side is the number of nearest-neighbor cations (6) multiplied by 2, necessary in order to take account of the total number of superexchange paths.

The two unknowns in Eq. (7), f and $k_2 J$, may be determined from any two measurements of T_f, say for $y = 0.03$ and $y = 0.15$. Calculation gives $f = 0.72$ and $k_2 J = 28$. Both these results are in accord with expectations based on the energy diagram. First, the interaction of the Fe^{3+} ions with the Mn^{4+}-Mn^{3+} system leads to a dilution that weakens $k_1 t$, that is, to a value of f less than unity. Second, the interaction between like ions will be greater than between unlike ions, so that it is expected that $k_1 t > k_2 J$. The value of T_f obtained with the above parameters for $x = 0.10$ agrees exactly with the experimental value.

For $x = 0.44$, and $y = 0$, Eq. (6) yields $k_1 t = 58$. Then, use of the values for f and $k_2 J$ obtained for $x = 0.30$ gives values for T_f that are listed in Table III. They are not as close to the experimental data as might have been hoped. Since $x = 0.44$ is close to the upper limit for ferromagnetism in the undoped compounds, the assumption that f is constant may not be valid.

The proposed energy diagram has implications concerning the electrical conductivity. Unfortunately, our samples are not suitable for such measurements. Since unenriched iron may be used, it may be possible in the future to grow good quality single crystals of the doped manganites and to determine the electrical transport properties.

CONCLUSIONS

The doping of the ferromagnetic manganites (LaPb)MnO_3 with iron dramatically alters the magnetic properties. The iron ions, which are in the high-spin ferric state, not only introduce an important antiferromagnetic superexchange interaction, but also lead to a substantial decrease in the double-exchange interaction. This decrease occurs both because the numbers of itinerant electrons are less, essentially a collective-electron effect, and because the transfer integral is reduced, primarily a localized-electron effect. Many iron ions have moments close to antiparallel to the manganese magnetization, but some, those with one or more iron ions as nearest neighbors, have

moments at about 55° to the manganese magnetization. The manganese system is also noncollinear; the magnetization is therefore decreased substantially. This mixed system, although complex, is a useful and interesting one for the study of the competition between collective and localized interactions.

ACKNOWLEDGMENTS

We wish to thank J. B. Goodenough and M. R. Spender for some helpful comments. This research was sponsored financially by the National Research Council and Defense Research Board of Canada.

---

*Present address: Dept. of Mathematics and Science, Hong Kong Polytechnic, Hung Hom, Kowloon, Hong Kong.

†Present address: Dept. of Chemistry, The University of Michigan, Ann Arbor, Mich. 48104.

[1]A. H. Morrish, B. J. Evans, J. A. Eaton, and L. K. Leung, Can. J. Phys. 47, 2691 (1969).

[2]L. K. Leung, A. H. Morrish, and C. W. Searle, Can. J. Phys. 47, 2697 (1969).

[3]C. W. Searle and S. T. Wang, Can. J. Phys. 48, 2023 (1970); K. Kubo and J. Ohata, J. Phys. Soc. Jpn. 33, 21 (1972).

[4]See, for example, C. Zener, Phys. Rev. 82, 403 (1951); P. W. Anderson and H. Hasegawa, *ibid.* 100, 675 (1955); and P. G. de Gennes, *ibid.* 118, 141 (1960).

[5]J. B. Goodenough, in *Progress in Solid State Chemistry*, edited by H. Reiss (Pergamon, New York, 1971), Vol. 5, pp. 145–399.

[6]Schwarzkopf Microanalytical Laboratory, Inc., New York, N. Y. 11377.

[7]B. J. Evans and L. K. Leung, Bull. Am. Ceram. Soc. 53, 344 (1974).